

Geophysical Research Letters®

RESEARCH LETTER

10.1029/2021GL096066

Seunghye Lee and Seohui Park equally contributed to the paper.

Key Points:

- Conventional aerosol data assimilation (DA) suffers from large uncertainties when using satellite aerosol optical depth (AOD) observations
- Machine learning was applied to estimate ground particulate matter (PM) concentrations from the satellite AOD for use in the conventional 3D-VAR DA system
- The modified DA experiment remarkably improves the PM₁₀ and PM_{2.5} prediction performance compared to the conventional AOD DA experiment

Supporting Information:

Supporting Information may be found in the online version of this article.

Correspondence to:

M.-I. Lee,
milee@unist.ac.kr





Citation:

Lee, S., Park, S., Lee, M.-I., Kim, G., Im, J., & Song, C.-K. (2022). Air quality forecasts improved by combining data assimilation and machine learning with satellite AOD. *Geophysical Research Letters*, 49, e2021GL096066. <https://doi.org/10.1029/2021GL096066>

Received 14 SEP 2021
Accepted 23 DEC 2021

© 2021. American Geophysical Union.
All Rights Reserved.

Air Quality Forecasts Improved by Combining Data Assimilation and Machine Learning With Satellite AOD

Seunghye Lee¹ , Seohui Park¹ , Myong-In Lee¹ , Ganghan Kim¹ , Jungho Im¹ , and Chang-Keun Song¹ 

¹Department of Urban and Environmental Engineering, Ulsan National Institute of Science and Technology, Ulsan, Korea

Abstract Satellite aerosol optical depth (AOD) data assimilation (DA) using numerical air quality forecast models has shown a limited improvement due to large uncertainties in the AOD observation operator. This study employed a machine learning (ML) algorithm to estimate the ground-level particulate matter (PM) from the Geostationary Ocean Color Imager (GOCI) AOD through the random forest with high accuracy. Analysis fields were subsequently produced by applying PM estimations to the Weather Research and Forecasting-Chemistry/three-dimensional variational DA system. Initialization of the model with the new analysis remarkably reduced the analysis error and increased the forecast skill. The PM₁₀ prediction showed significant benefits for up to 24 forecast hours, whereas PM_{2.5} prediction was improved for up to six forecast hours. Considering a broad spatial coverage by satellites, the synergistic use of DA and ML can maximize the effectiveness of satellite DA for air quality forecasts at the ground.

Plain Language Summary Due to their broad spatial coverage, satellite aerosol observations (OBS) are now widely used in real-time air quality monitoring and forecasts. A conventional method in most operational air quality monitoring and forecast centers uses satellite data to fill the spatiotemporal gap in the ground OBS network by combining them with the simulation data from the numerical air quality model. However, this process contains significant intrinsic errors in transforming aerosol products from satellites into the mass concentration values to be predicted. This study suggests using a machine-learning (ML) algorithm to estimate the ground-level particulate matter (PM) concentrations from the satellite optical data. This method not only covers broad geographical areas, including mountainous and oceanic regions that are not being covered by ground OBS stations but also improves the initialization process of the numerical air quality forecast model. The PM₁₀ prediction shows significant benefits for up to 24 forecast hours, whereas PM_{2.5} prediction is improved for up to six forecast hours. Considering a broad spatial coverage by satellites, the synergistic use of data assimilation (DA) and ML can maximize the effectiveness of satellite DA for air quality forecasts at the ground.

1. Introduction

Atmospheric aerosols have a profound impact on air quality, climate change, and human health (Forster et al., 2007; Lee et al., 2020). Numerical models can be used to provide accurate aerosol forecasting; however, there are certain challenges associated with numerical model forecasts, such as considerable uncertainties associated with the initial conditions (ICs), the physical and chemical parameterizations of the model, and the prescribed ground emissions. In this respect, data assimilation (DA) methods have been widely used to reduce uncertainty in ICs; a combination of observations (OBS) and model forecasts provides the best analysis (Seo et al., 2021; Yin et al., 2021).

With the rapid expansion of observing networks, previous studies indicate the improvement in the air quality forecasts by assimilating aerosol optical depth (AOD) retrievals from geostationary and polar-orbiting satellites (Choi et al., 2020; Liu et al., 2011; Pope et al., 2016; Saide et al., 2014; Xia et al., 2019) as well as surface particulate matter (PM) OBS (Feng et al., 2018; Pagowski & Grell, 2012). Although in situ surface PM OBS provide the best quality data, they only relate to a limited area, whereas satellite AOD retrievals cover a broad geographical range at a high spatial resolution. However, predictions for surface PM concentration with the assimilation of AOD have not yet attained a practical level of accuracy despite advances in the skill of applying AOD made in previous studies. Mostly the forecast skill for PM₁₀ or PM_{2.5} has increased for the daily averaged values (Saide et al., 2014),

but it is a common problem to exhibit a quick degradation of the forecast accuracy during the initial few hours of the forecast (Pang et al., 2018; Schwartz et al., 2012).

Machine learning (ML) methods have recently become popular with respect to their usage in air quality forecasts (Bai et al., 2019; Xiao et al., 2020). However, they have difficulties representing the spatial distributions of PM concentrations as point-based ground OBS. And they only show a high predictive power on a daily scale; their performance on an hourly scale is unsatisfactory. On the other hand, numerical (i.e., dynamical) models initialized from the conventional DA system are comprehensive in filling spatial gaps in the OBS and representing complicated interactions among various chemical and aerosol species consisting of PM. Recently, a few studies applied ML to the conventional aerosol DA system developed for the numerical models. For example, Jin et al. (2019) discovered that dust storm DA and forecasts were improved using a ML approach to correct the observation bias in dust prior to use in DA.

As previously mentioned, current predictions exhibit a rapid decline in accuracy for the initial few hours. This is primarily due to large errors in the initial analysis fields when assimilating the AOD and is related to the nonlinear relationship between the satellite-based total column AOD and in-situ PM concentrations (Kim et al., 2021; Wang et al., 2017), even though specified model background error statistics in the DA system provide vertical dependence in distributing innovation (i.e., observation minus model background). Another problem, which is seemingly more critical but has not received the same amount of focus in previous literature, originates from the uncertainty in the AOD observation operator, which converts the mass concentration of each aerosol species from the model background to the optical signal of AOD at the observation locations. The operator is subject to considerable uncertainty due to many associated assumptions and empirical parameters, such as the aerosol size distribution and single scattering albedo inside the radiative transfer model in the forecasting system (Lee et al., 2016; Ma et al., 2020). Therefore, with the aim of alleviating this problem, this study replaces the satellite-derived AOD with PM concentrations that are not obtained from in-situ PM OBS but are estimated by the ML algorithm using the AOD data. Using a relatively more certain PM operator instead of a highly uncertain AOD operator could reduce observation errors and provide better initial fields.

This study, therefore, aims to improve the forecasting ability of PM_{10} and $PM_{2.5}$ by a novel approach combining ML (i.e., Random Forest (RF)) and DA (i.e., 3D-VAR) over East Asia in April–May 2019. The study comprises two parts: a) the estimation of satellite-based PM concentrations through the ML (i.e., RF) approach, and b) the evaluation of PM forecasting models started from the DA analysis updated by the satellite-based PM. The data and methods are presented in Section 2, the results and discussion are given in Section 3, and Section 4 provides conclusions.

2. Data and Methods

The AOD is one of the key parameters used to estimate surface PM. This study obtained the Geostationary Ocean Color Imager (GOCI) AOD products processed by the Yonsei aerosol retrieval version 2 (Choi et al., 2018), which cover East Asia (113.4–146.6 E, 24.75–47.25 N) with a 6×6 km horizontal resolution. As the AOD signal is obtained by the visible channel, GOCI AODs are provided hourly for 8 hr (00–07 UTC) each day. Observed hourly PM_{10} and $PM_{2.5}$ concentrations were collected by AirKorea in South Korea, the Beijing Municipal Environmental Protection Monitoring Center in China, and the National Institute for Environmental Studies in Japan. These data were used as reference data to the ML algorithm and verify the forecasting skill using the numerical model.

This study applied RF to the real-time learning approach, which conducts PM modeling every hour to increase the accuracy of ambient PM concentrations (hereafter referred to as the RF model). RF is not significantly affected by multicollinearity between input variables (Quach, 2012). Compared to other ML and deep learning methods, RF is fast and has high performance, and can provide spatial distribution (Shin et al., 2020). The RF model was built by accumulating training samples for the past 30 days, including now-states; the model was updated every hour from 00 to 07 UTC when the GOCI AOD was available. Note that the 30-day time window was determined arbitrarily to account for short- and long-term variation, but the calibration and validation results were not significantly different when the window size was reduced to 20 or 10 days. Validation of the RF model was conducted in the spatial domain. The stations aggregated in each grid were randomly divided as follows: 85% for calibration (1,719 stations) and 15% for validation (304 stations), and their locations are shown in Figure S1. Validation samples

were not included in the RF model development. In addition, the forecast performance of the numerical model was verified for the 85% and 15% regions, respectively. The input data, preprocessing, and other details in the RF model refer to the supporting information Text S1. The data used in this study are summarized in Table S1.

The satellite DA was performed using the Grid-point Statistical Interpolation (GSI) 3D-VAR system (Kleist et al., 2009). The 3D-VAR system optimizes the model state vector (x) by minimizing a cost function (J) that considers both model and observation errors. The cost function is given by

$$J(x) = \frac{1}{2} [(x - x_b)^T \mathbf{B}^{-1} (x - x_b) + (y - H(x))^T \mathbf{R}^{-1} (y - H(x))] \quad (1)$$

where x_b is the background vector, y is the observation vector, \mathbf{B} and \mathbf{R} represent the background and observation error covariance matrices, and H denotes the observation operator. Details of specifying background and observation errors refer to the Text S2 in Supporting Information S1.

When the 3D-VAR assimilates the satellite AOD directly in Equation 1, the AOD observation operator H in the GSI system uses the Community Radiative Transfer Model to calculate the AOD value from the vertical profiles of mass concentration for each aerosol species (Liu et al., 2011; Schwartz et al., 2012). The AOD (τ) for each aerosol type i at the j th model layer for a wavelength, λ , is calculated as

$$\tau_{ij}(\lambda) = \alpha(\lambda, i, r_{eff}) \cdot c_{ij} \quad (2)$$

where the mass extinction coefficient, α ($\text{m}^2 \text{g}^{-1}$), is calculated using the Mie scattering code (Hulst & van de Hulst, 1981), and c_{ij} is the aerosol layer mass in g m^{-2} . The effective radius (r_{eff}) of the aerosol variables is determined by assuming spherical aerosol particles and log-normal size distributions. However, the parameterization of α contains considerable uncertainty in the aerosol–radiation interaction. In Equation 1, the innovation, I , from the AOD OBS (y_{AOD}) is determined as

$$I = y_{AOD} - H_{AOD}(x) \quad (3)$$

and the AOD observation operator (H_{AOD}) was used in the control experiment. In the new experiment, the innovation was replaced with

$$I' = y'_{PM} - H_{PM}(x), \quad (4)$$

where y'_{PM} is the estimated PM OBS from the satellite AOD by the RF model, and H_{PM} is the PM observation operator.

The WRF-Chem version 3.9.1 (Grell et al., 2005) was used as the forward model to produce the model background (forecasts). The domain and configuration of the model refer to Text S2 in Supporting Information S1 and Figure S1. Three parallel analysis–forecast experiments were designed (Figure S2): one experiment served as the control run and employed no DA (hereafter NoDA). The second experiment is the conventional 3D-VAR DA run which assimilated the original GOCI AOD (hereafter CDA), and the third is the combined ML and 3D-VAR DA run which assimilated the surface PM derived from GOCI AOD by RF ML (hereafter MLDA). All experiments were conducted from April 1 to 31 May 2019. The 3D-VAR analysis was conducted at 00 and 06 UTCs because AOD OBS are only made during the daytime. A series of forecasts were started at each analysis time and ran for 24 hr. The performance was evaluated based on the Pearson correlation (R), mean bias (MB), root-mean-squared error (RMSE), and the relative RMSE (rRMSE) between OBS and simulations. The statistical confidence interval was evaluated by the bootstrap method, where the original data were sampled randomly with replacement for 100,000 times and calculated the one standard deviation of R and RMSE values.

3. Results and Discussion

3.1. Satellite-Based PM Estimation

Ground-level PM_{10} and $\text{PM}_{2.5}$ concentrations were estimated every hour during the operational time of the GOCI satellite. The performance of the RF model was shown in Figure 1 (a, d) through scatter plots between the OBS and the estimations. When all samples were used, RF provided a high performance, with R of 0.99 and 0.98 and rRMSE of 11.33% and 13.42% for PM_{10} and $\text{PM}_{2.5}$, respectively (Figures 1a and 1d). This performance was

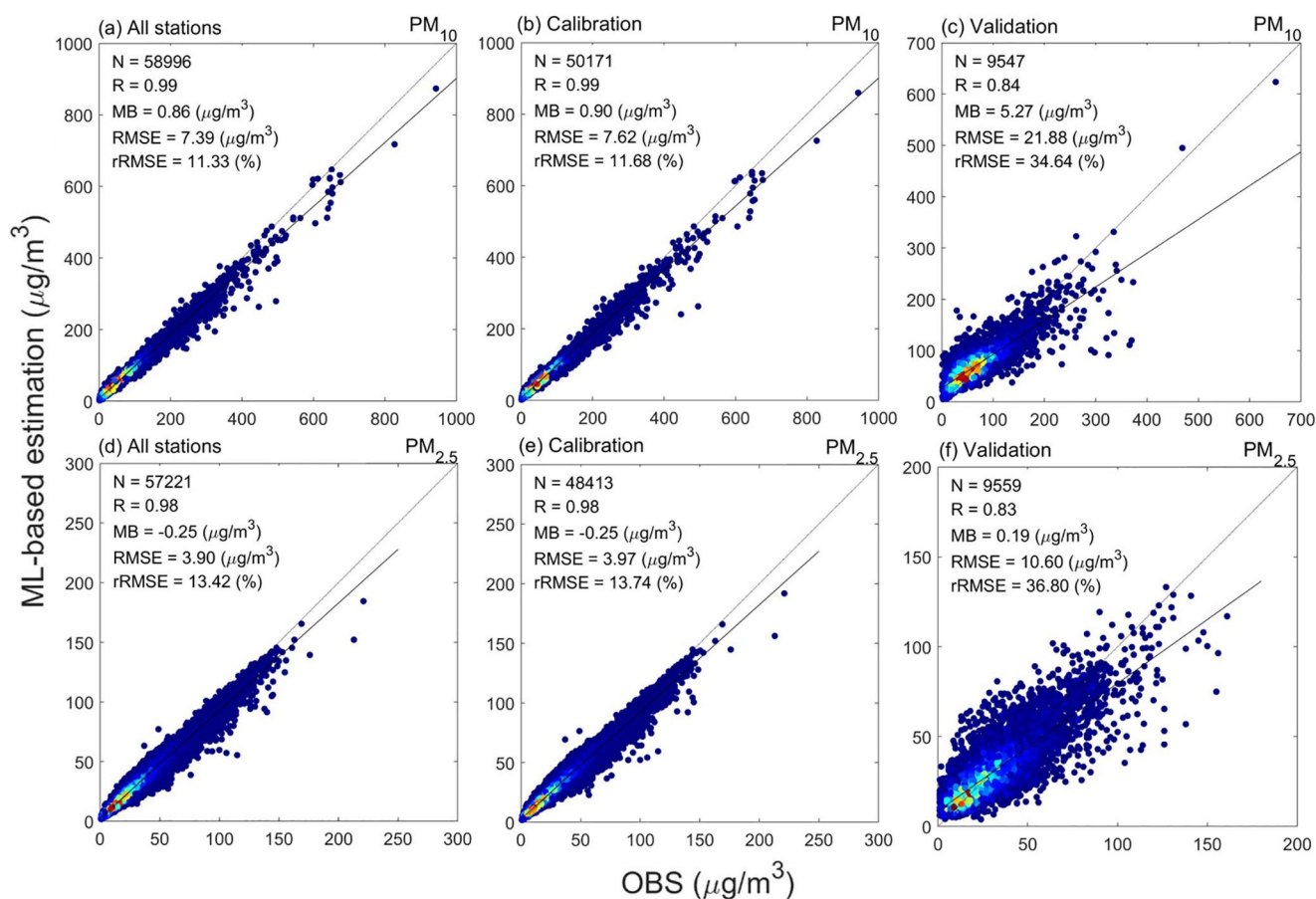


Figure 1. Scatterplots comparing observed and estimated (a–c) PM₁₀ and (d–f) PM_{2.5} for East Asia (a), (d) presents the RF model performance for all stations (b), (e) for the stations sampled for calibration (85%), and (c), (f) for the stations used in validation (15%). Each dot represents data samples for the entire analysis period of 8 times per day (00–07 UTC) and from April–May 2019. The lighter shades mean a higher point density. The dashed line represents the 1:1 diagonal line, and the solid line represents the slope of the linear regression line. The total number of data samples, the Pearson correlation (R), mean bias (MB), root-mean-squared error ($RMSE$), and the relative $RMSE$ ($rRMSE$) are shown in the upper left in each panel.

comparable to the calibration results (Figures 1b and 1e). The validation results also provided good performance, with R of 0.84 and 0.83 and $rRMSE$ of 34.64% and 36.80% for PM₁₀ and PM_{2.5}, respectively (Figures 1c and 1f). These validation results represent the performance of the RF model with satellite AOD for spatially unmeasured areas for ground PM concentrations, which is still high and comparable with that of previous ML studies (Jiang et al., 2021; Li et al., 2017; Liu et al., 2019). The RF model was not subject to data sampling after our additional 10-fold cross-validation test. The ranking of variable importance identified by the RF model when using all samples is shown in Figure S3. Hour of day, maximum wind speed, precipitation, and AOD were the most important input variables for both PM₁₀ and PM_{2.5}, consistent with those of previous RF studies (Park et al., 2019, 2020).

3.2. Data Assimilation and Forecast Results

The accuracy of CDA and MLDA was compared with the OBS and NoDA for the time-averaged analysis of PM concentrations for Domains one and two in Figure 2. The OBS (Figures 2a and 2e) showed that PM₁₀ and PM_{2.5} concentrations were higher in northern China and lower in South Korea. In a more detailed comparison of Domain 2, the OBS showed regional concentration variations in South Korea, with high concentrations in the northwestern metropolitan area and large cities on the southeastern coast. The NoDA experiment (Figures 2b and 2d) provided primarily negative biases for PM₁₀ and PM_{2.5} in northern China, South Korea, and especially in Manchuria, indicating that the WRF-Chem model underestimated PM. The CDA assimilated the satellite AOD and solved the underestimation of PM₁₀ in South Korea and Manchuria to some extent, but PM₁₀ concentrations were still underestimated in South Korea. In addition, the CDA exaggerated PM₁₀ in the Jing-Jin-Ji (JJJ) area in

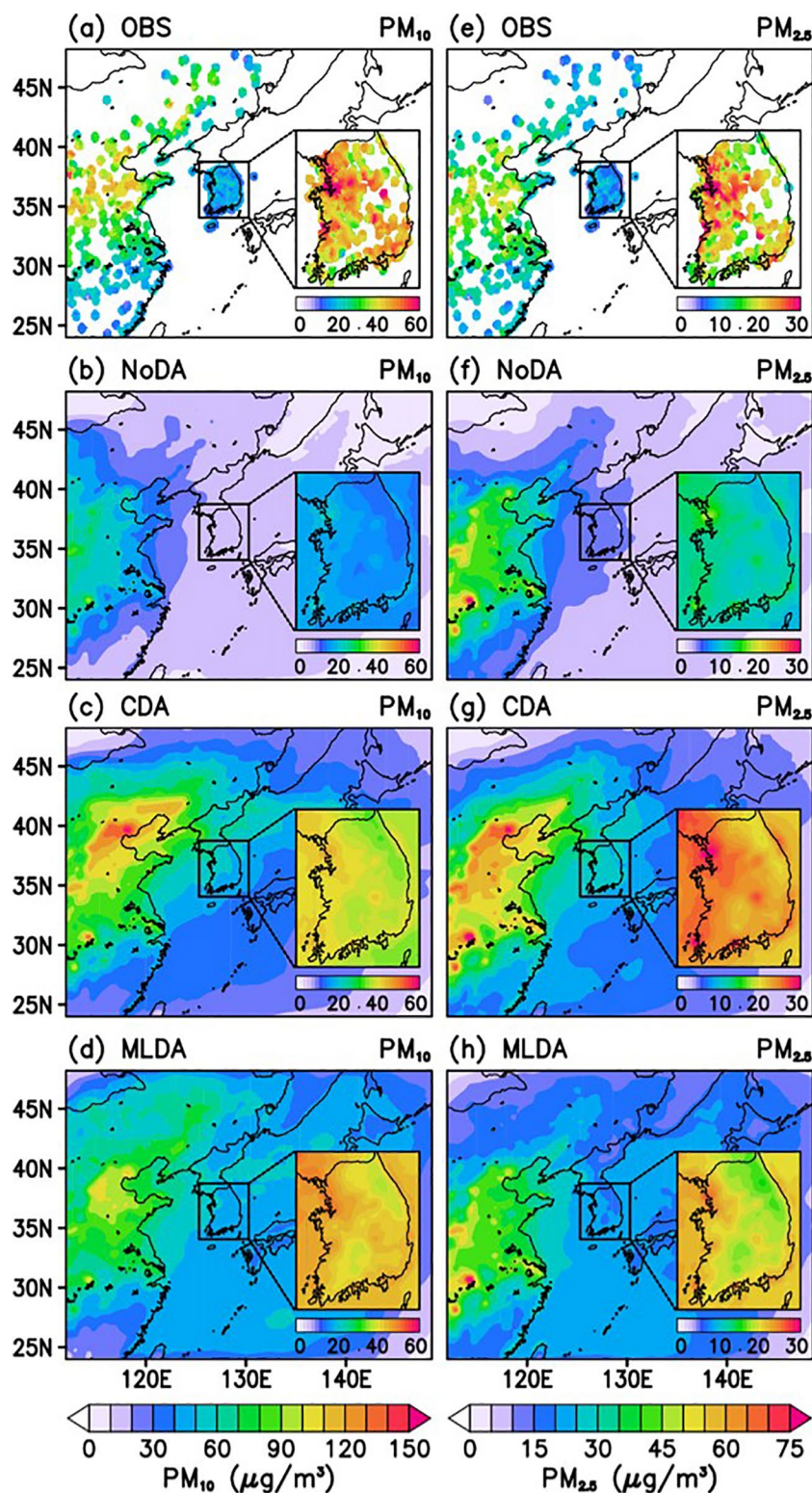


Figure 2. Spatial distributions of time-averaged PM_{10} (left column) and $PM_{2.5}$ (right column) mass concentrations ($\mu g m^{-3}$) at ground level during April and May 2019 from (a), (e) observations (b), (f) NoDA run (c), (g) CDA run, and (d), (h) MLDA run for Domain 1. The inner box in each panel shows the results over South Korea for Domain 2. The average surface PM mass concentrations were aggregated over all 00 and 06 UTCs for Domains 1 and 2 to verify the analysis fields.

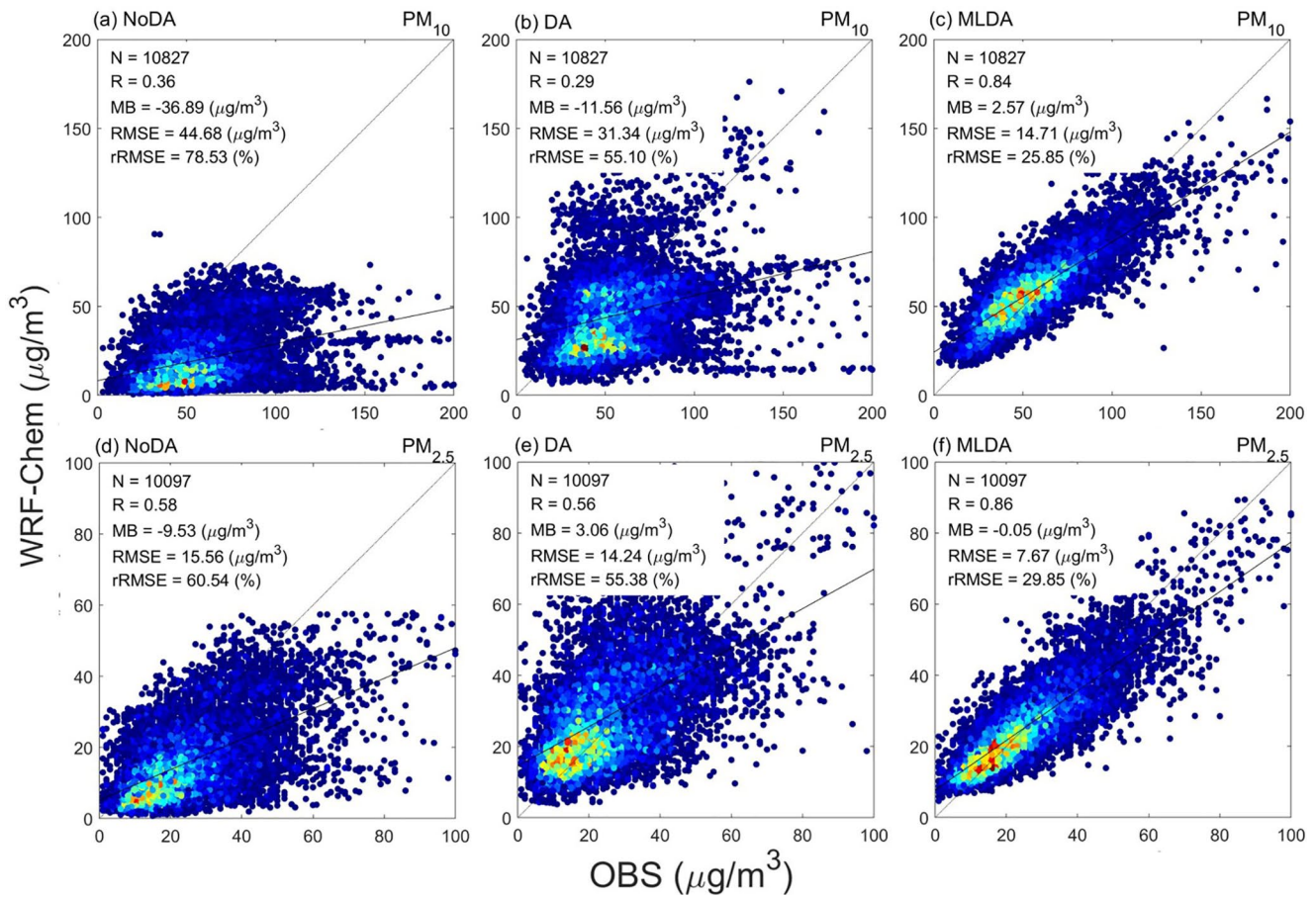


Figure 3. Scatter plots between the observed and the simulated surface PM_{10} (a–c) and $\text{PM}_{2.5}$ (d–f) for (a), (d) NoDA (b), (e) CDA, and (c), (f) MLDA. Each dot represents data samples over South Korea for all 00 and 06 UTCs in DA analyses fields from April–May 2019. The lighter shades mean a higher point density. The model PM output at the lowest vertical level was assumed to correspond with the surface AirKorea observation, and the model output was interpolated to the locations of the AirKorea sites for verification.

China. There was a similar overestimation for $\text{PM}_{2.5}$ in the region. The AOD DA is known sometimes to overestimate ground $\text{PM}_{2.5}$, as found in several prior studies (Feng et al., 2016; Ma et al., 2020). Ma et al. (2020) suggested that the dry humidity bias of the forecast models in the planetary boundary layer should adjust the ground PM concentration overly when the observed AOD is directly assimilated. As a result, there is a discrepancy in the ground PM concentration, indicating a nonlinear relationship between AOD and ground PM concentration due to the hygroscopic growth of aerosols.

The distribution of MLDA was the most similar to the observation. The spatial distributions of PM_{10} and $\text{PM}_{2.5}$ were improved over the JJJ area, where the CDA overestimated the values. In South Korea, the underestimated PM_{10} concentration and the overestimated $\text{PM}_{2.5}$ in CDA were resolved and became more consistent with the observed by MLDA. In summary, compared with directly assimilating AOD, assimilating the estimated ground PM concentration converted from GOCI AOD improved the quality of the ground PM analysis fields.

For a more objective verification, the scatter plots of PM_{10} and $\text{PM}_{2.5}$ were compared against AirKorea OBS in South Korea (Figure 3). Both CDA and MLDA showed an improvement over NoDA. CDA improved the analysis of PM_{10} and $\text{PM}_{2.5}$ with reduced RMSEs, compared to NoDA. However, although the negative MB of PM_{10} was improved, it was undercorrected with a negative bias. In contrast, the MB of $\text{PM}_{2.5}$ grew with a positive bias (as shown in Figure 2g). Therefore, the RMSE was not significantly improved in CDA, and the correlation showed no significant changes in CDA for both PM_{10} and $\text{PM}_{2.5}$. This suggests a fundamental difficulty in directly assimilating satellite AODs to initialize ground PM concentrations of the numeral forecast model. In contrast, MLDA

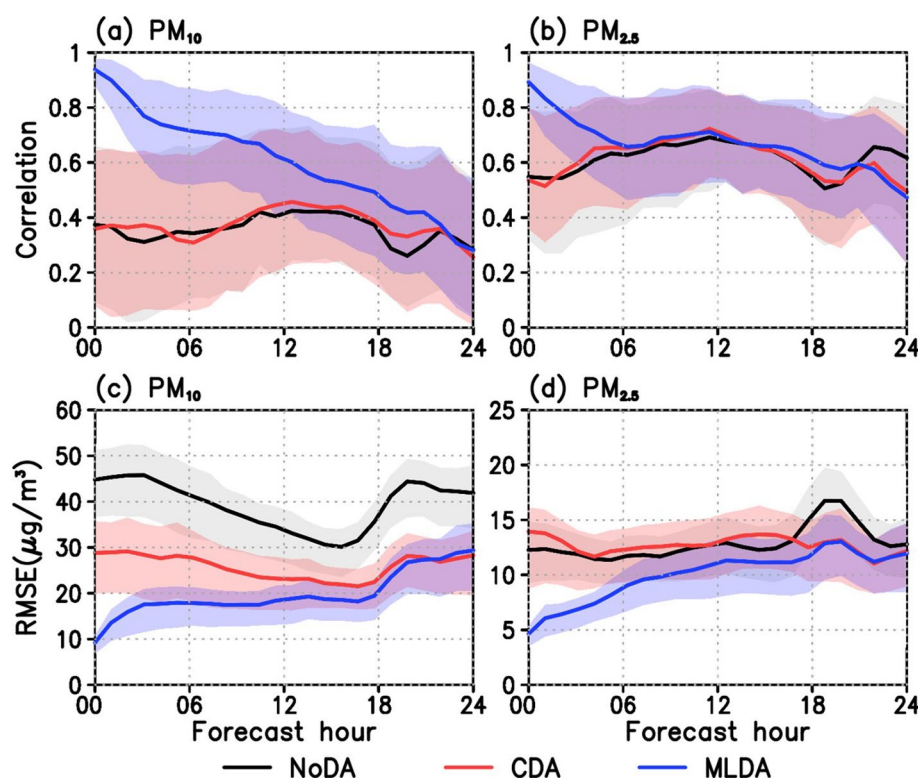


Figure 4. Correlation changes in the surface (a) PM_{10} and (b) $\text{PM}_{2.5}$ forecasts started at 06 UTC for each experiment. (c) and (d) show the RMSE changes for the PM_{10} and $\text{PM}_{2.5}$ forecasts, respectively. The colored shading indicates the variability of the correlation coefficient and RMSE shown as one standard deviation value calculated by 100,000 times of bootstrap. PM concentrations were first averaged for 16 provinces of South Korea before calculating R and RMSE and averaging for all provinces. The correlation coefficients and RMSEs were calculated for PM_{10} and $\text{PM}_{2.5}$ aggregated over all 06 UTC forecasts to assess the forecast skill from April–May 2019. Note that the 00 UTC forecasts (not shown) were inferior to the 06 UTC forecasts due to the less accurate ICs produced by RF. The real-time training with more weights in the recent data in the current RF algorithm was mainly responsible for the degraded training performance at 00 UTC, as the GOCI AOD is available from 00 to 07 UTCs.

significantly improved the MB, RMSE, rRMSE, and correlation of PM_{10} and $\text{PM}_{2.5}$, compared to NoDA and CDA. The improvement was particularly more prominent for PM_{10} than for $\text{PM}_{2.5}$.

Figure 4 compared the PM forecast performance in South Korea when the WRF-Chem was initialized by NoDA, CDA, and MLDA, respectively. Despite the overall reduction of RMSE for all forecast hours (Figures 4c and 4d), particularly in PM_{10} , no significant improvements in PM_{10} prediction skills measured by correlation were seen in the CDA experiment, compared to NoDA (Figure 4a). The correlation for NoDA and CDA remained less than 0.5 even at the initial forecast hour. Similar to PM_{10} , there were no significant differences between the $\text{PM}_{2.5}$ forecast by CDA and NoDA (Figure 4b). One difference was that the correlation was as high as 0.5–0.6 throughout the 24hr forecast.

MLDA substantially improved the accuracy of ICs of PM_{10} and $\text{PM}_{2.5}$ compared with CDA, as indicated at the 06 forecast hour with the correlation and RMSE. The correlation (Figures 4a and 4b) decreased and gradually approached NoDA as the forecast time increased. The forecast error measured by RMSE (Figures 4c and 4d) increased in time due to the errors in emissions and model processes (Kahnert, 2008). The DA effect of MLDA was maintained for more than 24 hr for PM_{10} and within 6 hr for $\text{PM}_{2.5}$. The reason for the relatively short effect in $\text{PM}_{2.5}$ seems to be due to the high basic predictability of $\text{PM}_{2.5}$.

The results above showed that MLDA significantly contributed to improving the forecast performance of ground PM concentrations. MLDA provided additional advantages because it improved the performance by minimizing the observation error in the cost function based on the nonlinear relationship between satellite AOD and ground PM. Considering that most ground PM stations are concentrated within inland, urban, and human residential areas and there are no PM OBS in areas such as oceans and mountains, satellite aerosol data can be used to overcome these

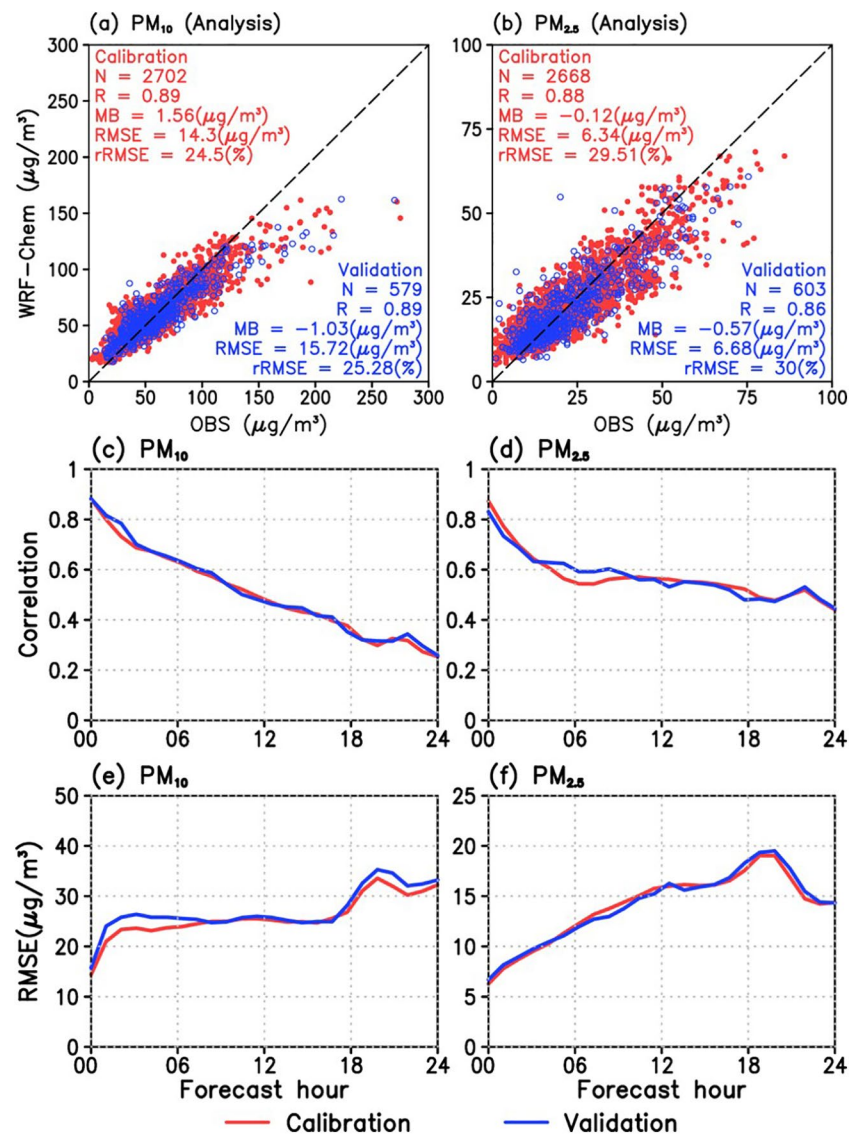


Figure 5. Scatter plots of simulated versus observed surface (a) PM_{10} and (b) $PM_{2.5}$ aggregated over all 06 UTC analyses from calibration sites (red) and validation sites (blue) over South Korea for April and May 2019 (c, d, e, f). Similar to Figure 4, but for calibration and validation runs.

limitations in spatial coverage. Our results showed the possibility of obtaining PM forecasts over more expansive areas, and additional analyses were conducted to verify this possibility. We analyzed the impacts of the 3D-VAR DA with the satellite and RF-estimated PM concentrations in the hypothetical unmeasured area for ground PM concentration. As this study used 85% of the PM stations for calibrating the RF model and reserved 15% for verification purposes as independent OBS, the evaluation of the PM forecast skill for those validation sites could help investigate the impacts in the areas lacking PM stations. The scatter plots of the calibration and the validation sets (Figures 5a and 5b) suggest that the overall accuracy of the validation set was lower than that of the calibration set, but the difference was not significant. Similar results were shown for PM forecasts. Although the validation set started with a slightly lower correlation (Figures 5c and 5d) and higher RMSE (Figures 5e and 5f) than the calibration set in both PM_{10} and $PM_{2.5}$, they are statistically inseparable throughout the 24hr forecast. The correlations of PM_{10} (Figure 5c) and $PM_{2.5}$ (Figure 5d) were maintained above 0.5 for up to 12 forecast hours in both the calibration and validation sets. This result proves that the geographical limitations of ground stations can be significantly improved via MLDA.

Another interesting point is that the calibration set tended to slightly decrease the correlation and increase RMSE compared to the RF results after DA; however, the validation set improved the correlation and RMSE values

after DA compared to RF (Figures 5a and 5b, and Figure S4). For example, the correlation for the validation sets increased from 0.87 and 0.82 in RF to 0.89 and 0.86 in MLDA for PM_{10} and $PM_{2.5}$, respectively. The RMSE was also reduced accordingly. The RF result showed the overfitting problem in Figure S4, where the validation set has a lower accuracy than the calibration set. In the areas lacking PM stations, we found that the MLDA results solved the overfitting problem of ML through 3D-VAR DA; both observation and model errors were considered, and the forecast results were more accurate than the RF results.

4. Conclusions

The DA using satellite AOD is widely used to initialize PM forecasts because of its higher spatiotemporal resolution compared with ground PM OBS. However, there are certain limitations in using satellite AOD for improving PM prediction skills because of the non-linearity between AOD and ground PM concentrations and the inherent large uncertainties of the AOD operators. This study combined the 3D-VAR DA system with the RF ML approach (MLDA) to improve air quality predictions over South Korea. First, RF was applied to estimate ground PM_{10} and $PM_{2.5}$ concentrations from GOCI AOD, which covered a broader area with very high accuracy. Next, the 3D-VAR DA with the estimated PM provided a more realistic spatiotemporal variation of ground PM concentration than the conventional DA with GOCI AOD, therefore improving the quality of the initial field for the aerosol forecast model significantly compared to the conventional DA system.

The MLDA experiment showed a high improvement effect (with an R reaching 0.9) for both PM_{10} and $PM_{2.5}$ at the time of assimilation, and the forecast improvement remained for over 24 hr for PM_{10} and up to 6 hr for $PM_{2.5}$. The effect of MLDA was more pronounced in PM_{10} than in $PM_{2.5}$, and this is considered to be related to the low predictability of PM_{10} . The potential benefit of MLDA was highlighted in the areas of hypothetical unmeasured areas for ground PM concentration through investigating with the independent validation OBS. This study proves that the prediction of PM concentrations can be significantly improved using this method, even in areas lacking ground observation stations.

One of the limitations in this study is the missing values in AOD over the cloudy area, which prevents ML from estimating PM concentration. The ML algorithm applicable to all sky conditions will help improve the spatial coverage for the PM estimation from satellites such as in the long-range transport events following the synoptic storms. Although this study examined the model performance only for spring, East Asian monsoon drives pronounced seasonal changes in regional weather and circulation, as well as local emission and long-range transport. More rigorous tests for other seasons have remained for future study.

Data Availability Statement

The WRF-Chem model version 3.9.1 is available on https://www2.mmm.ucar.edu/wrf/users/download/get_sources.html#WRF-Chem. FNL data which was used LBCs and ICs for the meteorological fields of WRF-Chem can be found at <http://rda.ucar.edu/datasets/ds083.2/>. The EDGAR-HTAP emission inventory is available at <https://www.acom.ucar.edu/wrf-chem/download.shtml>. The RF model used the randomforestregressor of sklearn ensemble library in python. The surface PM_{10} and $PM_{2.5}$ observational data are downloaded from the Beijing Municipal Environmental Protection Monitoring Center (<https://beijingair.sinaapp.com/>; Only available in Chinese) for China using open Application Programming Interface (e.g., https://quotsoft.net/air/data/china_sites_20190401.csv) and the National Institute of Environmental Research AirKorea website (https://www.airkorea.or.kr/web/last_amb_hour_data?pMENU_NO=123; Only available in Korean) for South Korea. The Geostationary Ocean Color Imager (GOCI) AOD Yonsei aerosol retrieval (YAER) version 2 data are available upon request to Choi et al. (2018). The input data for RF model such as the GOCI AOD are available at a Zenodo repository (<https://doi.org/10.5281/zenodo.5499010>).

References

- Bai, Y., Zeng, B., Li, C., & Zhang, J. (2019). An ensemble long short-term memory neural network for hourly $PM_{2.5}$ concentration forecasting. *Chemosphere*, 222, 286–294. <https://doi.org/10.1016/j.chemosphere.2019.01.121>
- Choi, M., Kim, J., Lee, J., Kim, M., Park, Y.-J., Holben, B., et al. (2018). GOCI Yonsei aerosol retrieval version 2 products: An improved algorithm and error analysis with uncertainty estimation from 5-year validation over East Asia. *Atmospheric Measurement Techniques*, 11(1), 385–408. <https://doi.org/10.5194/amt-11-385-2018>

Acknowledgments

This research was supported by the FRIEND (Fine Particle Research Initiative in East Asia Considering National Differences) Project through the National Research Foundation of Korea (NRF) funded by the Ministry of Science and ICT (Grant No: 2020M3G1A1114615). The model simulations were performed by using the supercomputing resource of the Korea Meteorological Administration (National Center for Meteorological Supercomputer). The authors thank Myungje Choi and Jhoon Kim from Yonsei University for providing GOCI AOD data.

- Choi, Y., Chen, S. H., Huang, C. C., Earl, K., Chen, C. Y., Schwartz, C. S., & Matsui, T. (2020). Evaluating the impact of assimilating aerosol optical depth observations on dust forecasts over North Africa and the East Atlantic using different data assimilation methods. *Journal of Advances in Modeling Earth Systems*, 12(4), e2019MS001890. <https://doi.org/10.1029/2019ms001890>
- Feng, S., Jiang, F., Jiang, Z., Wang, H., Cai, Z., & Zhang, L. (2018). Impact of 3DVAR assimilation of surface PM_{2.5} observations on PM_{2.5} forecasts over China during wintertime. *Atmospheric Environment*, 187, 34–49. <https://doi.org/10.1016/j.atmosenv.2018.05.049>
- Feng, Y., Cadeddu, M., Kotamarthi, V., Renju, R., & Raju, C. S. (2016). Humidity bias and effect on simulated aerosol optical properties during the Ganges Valley Experiment. *Current Science*, 111, 93–100. <https://doi.org/10.18520/cs/v111/i1/>
- Forster, P., Ramaswamy, V., Artaxo, P., Berntsen, T., Betts, R., Fahey, D. W., et al. (2007). Changes in atmospheric constituents and in radiative forcing. In *Climate change 2007. The physical science basis*. Chapter 2.
- Grell, G. A., Peckham, S. E., Schmitz, R., McKeen, S. A., Frost, G., Skamarock, W. C., & Eder, B. (2005). Fully coupled “online” chemistry within the WRF model. *Atmospheric Environment*, 39(37), 6957–6975. <https://doi.org/10.1016/j.atmosenv.2005.04.027>
- Hulst, H. C., & van de Hulst, H. C. (1981). *Light scattering by small particles*. Courier Corporation.
- Jiang, T., Chen, B., Nie, Z., Ren, Z., Xu, B., & Tang, S. (2021). Estimation of hourly full-coverage PM_{2.5} concentrations at 1-km resolution in China using a two-stage random forest model. *Atmospheric Research*, 248, 105146. <https://doi.org/10.1016/j.atmosres.2020.105146>
- Jin, J., Lin, H. X., Segers, A., Xie, Y., & Heemink, A. (2019). Machine learning for observation bias correction with application to dust storm data assimilation. *Atmospheric Chemistry and Physics*, 19(15), 10009–10026. <https://doi.org/10.5194/acp-2019-298>
- Kahnert, M. (2008). Variational data analysis of aerosol species in a regional CTM: Background error covariance constraint and aerosol optical observation operators. *Tellus B: Chemical and Physical Meteorology*, 60(5), 753–770. <https://doi.org/10.3402/tellusb.v60i5.16960>
- Kim, G., Lee, S., Im, J., Song, C. K., Kim, J., & Lee, M. I. (2021). Aerosol data assimilation and forecast using Geostationary Ocean Color Imager aerosol optical depth and in-situ observations during the KORUS-AQ observing period. *GIScience and Remote Sensing*, 58(3), 1–20. <https://doi.org/10.1080/15481603.2021.1972714>
- Kleist, D. T., Parrish, D. F., Derber, J. C., Treadon, R., Wu, W.-S., & Lord, S. (2009). Introduction of the GSI into the NCEP global data assimilation system. *Weather and Forecasting*, 24(6), 1691–1705. <https://doi.org/10.1175/2009WAF2222201.1>
- Lee, S., Lee, M. I., Song, C. K., Kim, K. M., & da Silva, A. M. (2020). Interannual variation of the East Asia jet stream and its impact on the horizontal distribution of aerosol in boreal spring. *Atmospheric Environment*, 223, 117296. <https://doi.org/10.1016/j.atmosenv.2020.117296>
- Lee, S., Song, C. H., Park, R. S., Park, M. E., Han, K. M., Kim, J., et al. (2016). GIST-PM-Asia v1: Development of a numerical system to improve particulate matter forecasts in South Korea using geostationary satellite-retrieved aerosol optical data over northeast Asia. *Geoscientific Model Development*, 9, 17–39. <https://doi.org/10.5194/gmd-9-17-2016>
- Li, T., Shen, H., Yuan, Q., Zhang, X., & Zhang, L. (2017). Estimating ground-level PM_{2.5} by fusing satellite and station observations: A geo-intelligent deep learning approach. *Geophysical Research Letters*, 44(23), 11985–11993. <https://doi.org/10.1002/2017GL075710>
- Liu, J., Weng, F., & Li, Z. (2019). Satellite-based PM_{2.5} estimation directly from reflectance at the top of the atmosphere using a machine learning algorithm. *Atmospheric Environment*, 208, 113–122. <https://doi.org/10.1016/j.atmosenv.2019.04.002>
- Liu, Z., Liu, Q., Lin, H. C., Schwartz, C. S., Lee, Y. H., & Wang, T. (2011). Three-dimensional variational assimilation of MODIS aerosol optical depth: Implementation and application to a dust storm over East Asia. *Journal of Geophysical Research: Atmospheres*, 116(D23). <https://doi.org/10.1029/2011JD016159>
- Ma, C., Wang, T., Jiang, Z., Wu, H., Zhao, M., Zhuang, B., et al. (2020). Importance of bias correction in data assimilation of multiple observations over eastern China using WRF-Chem/DART. *Journal of Geophysical Research: Atmospheres*, 125(1), e2019JD031465. <https://doi.org/10.1029/2019JD031465>
- Pagowski, M., & Grell, G. A. (2012). Experiments with the assimilation of fine aerosols using an ensemble Kalman filter. *Journal of Geophysical Research: Atmospheres*, 117(D21). <https://doi.org/10.1029/2012JD018333>
- Pang, J., Liu, Z., Wang, X., Bresch, J., Ban, J., Chen, D., & Kim, J. (2018). Assimilating AOD retrievals from GOCI and VIIRS to forecast surface PM_{2.5} episodes over Eastern China. *Atmospheric Environment*, 179, 288–304. <https://doi.org/10.1016/j.atmosenv.2018.02.011>
- Park, S., Lee, J., Im, J., Song, C.-K., Choi, M., Kim, J., et al. (2020). Estimation of spatially continuous daytime particulate matter concentrations under all sky conditions through the synergistic use of satellite-based AOD and numerical models. *The Science of the Total Environment*, 713, 136516. <https://doi.org/10.1016/j.scitotenv.2020.136516>
- Park, S., Shin, M., Im, J., Song, C.-K., Choi, M., Kim, J., et al. (2019). Estimation of ground-level particulate matter concentrations through the synergistic use of satellite observations and process-based models over South Korea. *Atmospheric Chemistry and Physics*, 19(2), 1097–1113. <https://doi.org/10.5194/acp-19-1097-2019>
- Pope, R., Marsham, J., Knippertz, P., Brooks, M., & Roberts, A. (2016). Identifying errors in dust models from data assimilation. *Geophysical Research Letters*, 43(17), 9270–9279. <https://doi.org/10.1002/2016GL070621>
- Quach, A. T. (2012). *Interactive random forests plots*.
- Saide, P. E., Kim, J., Song, C. H., Choi, M., Cheng, Y., & Carmichael, G. R. (2014). Assimilation of next generation geostationary aerosol optical depth retrievals to improve air quality simulations. *Geophysical Research Letters*, 41(24), 9188–9196. <https://doi.org/10.1002/2014GL062089>
- Schwartz, C. S., Liu, Z., Lin, H. C., & McKeen, S. A. (2012). Simultaneous three-dimensional variational assimilation of surface fine particulate matter and MODIS aerosol optical depth. *Journal of Geophysical Research: Atmospheres*, 117(D13). <https://doi.org/10.1029/2011JD017383>
- Seo, E., Lee, M.-I., & Reichle, R. H. (2021). Assimilation of SMAP and ASCAT soil moisture retrievals into the JULES land surface model using the Local Ensemble Transform Kalman Filter. *Remote Sensing of Environment*, 253, 112222. <https://doi.org/10.1016/j.rse.2020.112222>
- Shin, M., Kang, Y., Park, S., Im, J., Yoo, C., & Quackenbush, L. J. (2020). Estimating ground-level particulate matter concentrations using satellite-based data: A review. *GIScience and Remote Sensing*, 57(2), 174–189. <https://doi.org/10.1080/15481603.2019.1703288>
- Wang, W., Mao, F., Du, L., Pan, Z., Gong, W., & Fang, S. (2017). Deriving hourly PM_{2.5} concentrations from himawari-8 aods over beijing–tianjin–hebei in China. *Remote Sensing*, 9(8), 858. <https://doi.org/10.3390/rs9080858>
- Xia, X., Min, J., Wang, Y., Shen, F., Yang, C., & Sun, Z. (2019). Assimilating Himawari-8 AHI aerosol observations with a rapid-update data assimilation system. *Atmospheric Environment*, 215, 116866. <https://doi.org/10.1016/j.atmosenv.2019.116866>
- Xiao, F., Yang, M., Fan, H., Fan, G., & Al-Qaness, M. A. (2020). An improved deep learning model for predicting daily PM_{2.5} concentration. *Scientific Reports*, 10(1), 1–11, 20988. <https://doi.org/10.1038/s41598-020-77757-w>
- Yin, R., Han, W., Gao, Z., & Li, J. (2021). Impact of high temporal resolution FY-4A Geostationary Interferometric Infrared Sounder (GIIRS) radiance measurements on Typhoon forecasts: Maria (2018) case with GRAPES global 4D-Var assimilation system. *Geophysical Research Letters*, 48(15), e2021GL093672. <https://doi.org/10.1029/2021GL093672>